NANO, MESO, MICRO : SCIENCES ET INNOVATIONS POUR LA RADIO ET LA PHOTONIQUE.

Passive mode locking of MIR QCLs using graphene as a saturable absorber

A. Outafat[1,2], S. Faci[1], E. Richalot[2], S. Protat[2], C. Algani[1]

1. Univ Gustave Eiffel, CNRS, CNAM, ESYCOM, 292 Rue Saint-Martin, 75003 Paris

2. Univ Gustave Eiffel, CNRS, ESYCOM, F-77454 Marne-la-Vallée, France.

Mots clés (en français et en anglais) :
Laser à cascade quantique, Verrouillage de modes, Absorption saturable, Graphène.
Quantum Cascade Laser, Modelocked Laser, Saturable absorption, Graphene.

Résumé/Abstract

Le verrouillage de modes de laser à cascade quantique (QCLs) est l'un des grands chalenges à cause du faible temps de recouvrement de gain comparé aux lasers à semiconducteur. Ainsi, l'utilisation des techniques conventionnelles comme un absorbant saturable à base de matériaux semiconducteurs n'est pas une solution efficace. Dans cette communication, nous proposons l'étude d'une telle structure en intégrant une couche de graphène qui possède un temps de relaxation très court devant la largeur des impulsions générées et possède une intensité de saturation inférieure aux autres absorbants saturables. Les résultats de simulation avec la méthode FDTD ont permis de démontrer le verrouillage de modes passif de QCL moyen infrarouge.

Passive mode locking in quantum cascade lasers (QCLs) is one of great challenges because of the ultrafast relaxation time of QCL compared to conventional semiconductor lasers. Thus, the use of conventional saturable absorber as Semiconductor saturable-absorber mirror (SESAM) is not the best solution for QCLs mode locking. The study proposed in this paper concerns the use the single-layer graphene as a saturable absorber. The relaxation time in graphene is very fast compared to the pulse width and relaxation time of QCL and its saturation intensity is low compared to other saturable absorbers. The use of graphene with high reflection mirror allows to increase the internal electric field which easily reaches the graphene saturation level.

1 Introduction

Demonstrated for the first time in 1994 at bell labs [1], the QCL structure is based on multiple quantum wells (QW) with radiative transition appearing between two energy levels in the conduction band. This radiative transition is repeated N times and allow photon emission at energy much lower than traditional lasers can offer. QCL can operate from Mid-Infrared (MIR) to Far-Infrared (FIR) spectral region depending upon the number of QW periods and the used materials. Short pulses generation from MIR QCL in the spectral range 3 – 12 µm is one of the huge challenges since its first demonstration until today, because of its fast gain recovery time of a few picoseconds compared to the roundtrip time of 40-60 ps for a 2-3 mm laser cavity length. Mode locking is a method used to synchronize the cavity longitudinal modes either by passive [2] or active [3], [4] techniques. In this work, we study the passive mode locking MIR QCL ability by integrating a single-layer graphene as a saturable absorber. The light-matter interaction within the laser active region is described by the two-level Maxwell-Bloch equations and within the graphene layer by the Maxwell-Ampere equation. These equations are solved using the Finite-Difference Time-Domain (FDTD) method [5]. In previous works dealing with FDTD method applied to simulate passive mode locking of photonic structure integrating graphene, the thickness of graphene is considered as a single spatial step [6]. We use another efficient method for the graphene by considering a suitable method for a thin material layer [7]. We use for the simulation a 0.33nm-thickness graphene which is equivalent to a bilayer graphene thickness.

2 Structure Modeling

2.1 Quantum cascade laser

The QCL dynamic is considered with the tow-level atom system which describes the interaction between the light and nonlinear mater [8]. It is modeled by the coupled Maxwell's equations (1)-(2) and Bloch equation (3)-(5) as following:

$$\frac{\partial H_x}{\partial t} = -\frac{1}{\mu_0}\frac{\partial E_z}{\partial y} \tag{1}$$

$$\frac{\partial E_z}{\partial t} = -\frac{1}{\varepsilon}\frac{\partial H_x}{\partial y} - \frac{N\mu}{\varepsilon T_2}\rho_a + \frac{N\mu\omega_0}{\varepsilon}\rho_b - l_0 E_z \tag{2}$$

$$\frac{\partial \rho_a}{\partial t} = \omega_0 \rho_b - \frac{1}{T_2}\rho_a \tag{3}$$

$$\frac{\partial \rho_b}{\partial t} = -\omega_0\rho_a - \frac{1}{T_2}\rho_b + 2\frac{\mu E_z}{\hbar}\Delta \tag{4}$$

$$\frac{\partial \Delta}{\partial t} = -2\frac{\mu E_z}{\hbar}\rho_b - \frac{\Delta}{T_1} + I + D\frac{\partial^2 \Delta}{\partial^2 z} \tag{5}$$

where E_z is the electric field, H_x is the magnetic field, l_0 is the linear loss, ε is the dielectric constant, μ_0 is the vacuum permeability, ρ_a and ρ_b are the existence probability of an electron in state a and b respectively, a and b indexes correspond respectively to the ground and excited states, μ is the electric dipole moment of a two-energy level atom, Δ is the inversion population, T_1 is the excited-state lifetime and T_2 the dephasing time, $\hbar$ is the reduced Planck constant, ω_0 is the atomic transition frequency, D is the dispersion coefficient and I is pumping ratio.

In this Maxwell-Bloch derivation, the light is propagates following the y-axis and the electric field has a linear polarisation following z-axis.

2.2 Graphene layer

The light interaction with graphene layer can be considered either by Maxwell-Block equations, continuity equations or Maxwell equations. We use Maxwell equations to describe this dynamic by considering a nonlinear conductivity to model the light intensity dependence. The relations that describe the interaction of light in graphene layer is given by:

$$\frac{\partial H_x}{\partial t} = -\frac{1}{\mu_0}\frac{\partial E_z}{\partial y} \tag{6}$$

$$\frac{\partial E_z}{\partial t} = \frac{1}{\varepsilon}\frac{\partial H_x}{\partial z} - \frac{2\,n_s}{\varepsilon\eta_0}\sigma(I)E_z \tag{7}$$

Following the Drude model and the frequency value in MIR range, the conductivity ansatz is given as function of the absorption by [6]

$$\sigma(I) \approx \frac{2n_s}{\eta_0}\alpha(I) \tag{8}$$

with n_s is the refractive index of the graphene and η_0 is the wave impedance.

The nonlinear absorption of a saturable absorber is composed of linear and nonlinear terms. The linear term is called non saturable absorption α_{ns} and is estimated to be 70% in single-layer graphene. The nonlinear term which is referred by saturable absorption α_s describe the maximum absorption or unsaturated losses. It is close to 13% in single-layer graphene in MIR wavelengths. Then, the nonlinear absorption is intensity dependence and is defined following the two absorption terms by

$$\alpha(I) = \alpha_{ns} + \frac{\alpha_s}{1+\frac{I}{I_s}} \tag{9}$$

where I is the light intensity and I_s represents the saturation intensity of graphene estimated to be around 0.2 $MW\ cm^{-2}$ at 10 µm wavelength [9].

Then, we replace the conductivity term in equation (7) to build the nonlinear electric filed dynamic in single-layer graphene as:

$$\frac{\partial E_z}{\partial t} = \frac{1}{\varepsilon}\frac{\partial H_x}{\partial z} - \frac{2\, n_s}{\varepsilon \eta_0}\left(\alpha_{ns} + \frac{\alpha_s}{1+\left(\frac{E_z}{E_s}\right)^2}\right)E_z \tag{10}$$

3 Discretization of light-Mater equations for FDTD

The resolution of the differential equations is obtained with the finite-difference time-domain method. This method is based on Yee's scheme [10], [5] and can be applied to various complex structures. Recently, FDTD was used to simulate the dynamic of passive mode locking of a telecom diode laser [6] and a THz frequency comb QCL. The principle of this method consists of the discretization of space domain in multiple grids with a step Δy and time domain computation each Δt. The electric field is computed at $n\,\Delta t$ points while Bloch equations and the magnetic field are computed at $(n + 1/2)\,\Delta t$ points, with n is an integer. The implementation of this method is simpler with the weakly coupling approach where the Maxwell-Ampère equation (2) and Bloch equations (3)-(5) are separated in time [10]. This configuration is suitable for explicit scheme and the obtained results are similar to the one obtained with the heavy coupling method for the 1D-FDTD method.

The spatial and time steps are important parameters to guarantee the convergence and the stability of FDTD. A small value of Δy induces a strong hardware resource and a large value affects the convergence. The spatial step is determined from the light wavelength and fixed here to $\frac{\lambda}{200}$. The QCL wavelength is 6.2µm which give the spatial step $\Delta y = 31\ nm$.

The time step is determined from the Courant number stability following the form $\Delta t \leq \frac{\Delta y}{c}$, with c is the light speed in vacuum. We fixe this condition to the maximum limit.

3.1 Quantum cascade laser

The discretised Maxwell-Bloch equations for QCL are then:

$$H_{x_{m+\frac{1}{2}}}^{\,n+\frac{1}{2}} = H_{x_{m+\frac{1}{2}}}^{\,n-\frac{1}{2}} - \frac{\Delta t}{\mu_0 \Delta y}\left(E_{z_{m+1}}^{\,n} - E_{z_m}^{\,n}\right) \tag{11}$$

$$E_{z_m}^{\,n+1} = E_{z_m}^{\,n} - \frac{\Delta t}{\varepsilon\, \Delta y}\left[H_{x_{m+\frac{1}{2}}}^{\,n+\frac{1}{2}} - H_{x_{m-\frac{1}{2}}}^{\,n+\frac{1}{2}}\right] - \frac{\Delta t\, N\, \mu}{\varepsilon T_2}\rho_{a_m}^{\,n+\frac{1}{2}} + \frac{\Delta t\, N\, \mu \omega_0}{\varepsilon}\rho_{b_m}^{\,n+\frac{1}{2}} - \frac{\Delta t\, l_0}{2}\left(E_{z_m}^{\,n+1} + E_{z_m}^{\,n}\right) \tag{12}$$

$$\rho_{a_m}^{\,n+\frac{1}{2}} = \rho_{a_m}^{\,n-\frac{1}{2}} - \frac{\Delta t}{2\, T_2}\left[\rho_{a_m}^{\,n+\frac{1}{2}} + \rho_{a_m}^{\,n-\frac{1}{2}}\right] + \frac{\Delta t\, \omega_0}{2}\left[\rho_{b_m}^{\,n+\frac{1}{2}} + \rho_{b_m}^{\,n-\frac{1}{2}}\right] \tag{13}$$

$$\rho_{b_m}^{\,n+\frac{1}{2}} = \rho_{b_m}^{\,n-\frac{1}{2}} - \frac{\Delta t\, \omega_0}{2}\left[\rho_{a_m}^{\,n+\frac{1}{2}} + \rho_{a_m}^{\,n-\frac{1}{2}}\right] - \frac{\Delta t}{2\, T_2}\left[\rho_{b_m}^{\,n+\frac{1}{2}} + \rho_{b_m}^{\,n-\frac{1}{2}}\right] + \frac{\Delta t\, \mu}{\hbar}E_{z_m}^{\,n}\left[\Delta_m^{\,n+\frac{1}{2}} + \Delta_m^{\,n-\frac{1}{2}}\right] \tag{14}$$

$$\Delta_m^{\,n+\frac{1}{2}} = \Delta_m^{\,n-\frac{1}{2}} - \frac{\Delta t\, \mu}{\hbar}E_{z_m}^{\,n}\left[\rho_{b_m}^{\,n+\frac{1}{2}} + \rho_{b_m}^{\,n-\frac{1}{2}}\right] - \frac{\Delta t}{2T_1}\left[\Delta_m^{\,n+\frac{1}{2}} + \Delta_m^{\,n-\frac{1}{2}}\right] + \Delta t\, I + \frac{\Delta t}{\Delta y^2}\, D\, \left[\Delta_{m+1}^{\,n-\frac{1}{2}} - 2\,\Delta_m^{\,n-\frac{1}{2}} + \Delta_{m-1}^{\,n-\frac{1}{2}}\right] \tag{15}$$

where the index m refers to the spatial location and the index n refers to the time step.

3.2 Graphene

The single-layer graphene consists of a one atom thick carbon layer. This thickness is very small compared to the spatial step Δy. To consider this thin layer, we use Maloney's method [11]. In this method, the thickness of graphene is limited in a cell portion $d = \frac{L_g}{\Delta_y}$ and the rest of the cell is filled by SiO_2. This hybrid cell is followed by the Bragg grating as described in Figure 1. The conductivity σ_M of the graphene in the occupied cell part is given by:

$$\sigma_M(I) = d\ \sigma(I) \tag{16}$$

The permittivity of graphene layer depends also on its thickness as:

$$\varepsilon_M = \varepsilon_0 \varepsilon_{SiO_2}(1-d) + \varepsilon_0 \sqrt{n_s} d \tag{17}$$

with ε_{SiO_2} the relative permittivity of graphene.

From (10) and (12) we can write:

$$\frac{\partial E_z}{\partial t} = \frac{1}{\varepsilon_M}\frac{\partial H_x}{\partial z} - \frac{2\, d\, n_s}{\varepsilon_M \eta_0}\left(\alpha_{ns} + \frac{\alpha_s}{1+\left(\frac{E_z}{E_s}\right)^2}\right)E_z \tag{18}$$

The equations (6) and (18) are resolved by the classical FDTD method. The computation of the magnetic field at time step $\left(n+\frac{1}{2}\right)\Delta t$ requires the old value at time step $\left(n-\frac{1}{2}\right)\Delta t$ and the known electric filed at time step $n\,\Delta t$. This computation for the magnetic field is made for a spatial point $m+\frac{1}{2}$ and is given by (19). The electric field determined at time step $(n+1)\,\Delta t$ requires the old electric field value at time step $n\,\Delta t$ and the magnetic fields at time steps $\left(n-\frac{1}{2}\right)\Delta t$ and $\left(n+\frac{1}{2}\right)\Delta t$. However, the electric field at the right-side of expression (18) is considered by the mean value at these time steps. This computation is made for a spatial point m. The discretization of Maxwell equations is thus:

$$H_{x\,m+\frac{1}{2}}^{\,n+\frac{1}{2}} = H_{x\,m+\frac{1}{2}}^{\,n-\frac{1}{2}} - \frac{\Delta t}{\mu_0 \Delta y}\left[E_{z\,m+1}^{\,n} - E_{z\,m}^{\,n}\right] \tag{19}$$

$$E_{z\,m}^{\,n+1} = \frac{1}{B}\left[E_{z\,m}^{\,n} A - \frac{\Delta t}{\varepsilon_M\, \Delta y}\left(H_{m+\frac{1}{2}}^{n+\frac{1}{2}} - H_{m-\frac{1}{2}}^{n+\frac{1}{2}}\right)\right] \tag{20}$$

where $A = 1 - \frac{\Delta t\, d\, n_s}{\varepsilon_M \eta_0}\left[\alpha_{ns} + \alpha_s\left(1 + \frac{\left(\frac{E_{z\,m}^{\,n} + E_{z\,m}^{\,n+1}}{2}\right)^2}{E_s{}^2}\right)^{-1}\right]$ and

$$B = 1 + \frac{\Delta t\, d\, n_s}{\varepsilon_M\, \eta_0}\left[\alpha_{ns} + \alpha_s\left(1 + \frac{\left(\frac{E_{z\,m}^{\,n} + E_{z\,m}^{\,n+1}}{2}\right)^2}{E_s{}^2}\right)^{-1}\right]$$

The squared electric field in expression (20) in terms A and B make an indirect resolution with FDTD. Then, it is more suitable to use an additional method like predictor-corrector scheme to resolve the expression. We adopt the fixed-point method to determine the unknown electric field. This method is based on an iterative scheme suitable for solving nonlinear equations by numerical approximation of the root without need to a derivative function [12]. The expression (20) is discretised following the form

$$x = f(x) \tag{21}$$

where x is the solution or the root of the function $f(\mathrm{x})$ which can be written as:

$$x = \frac{C}{D}E_m^n - \frac{\Delta t}{\varepsilon_M\, D\, \Delta y}\left[H_{m+\frac{1}{2}}^{n+\frac{1}{2}} - H_{m-\frac{1}{2}}^{n+\frac{1}{2}}\right] \tag{22}$$

where $C = 1 - \frac{d\,\Delta t\, n}{\varepsilon_M \eta_0}\left[\alpha_{ns} + \frac{\alpha_s}{1+\left(\frac{E_m^n + x}{2E_s}\right)^2}\right]$ and $D = 1 + \frac{d\,\Delta t\, n}{\varepsilon_M \eta_0}\left[\alpha_{ns} + \frac{\alpha_s}{1+\left(\frac{E_m^n + x}{2E_s}\right)^2}\right]$

4 Simulation results

Figure 1 represents the structure of passive mode locking of MIR QCLs using graphene as a saturable absorber. The total length of the laser cavity is 2.6 mm, the single-layer graphene and the high reflecting mirror are positioned to the one facet to create a saturable absorber mirror integrating graphene (GSAM). This high reflecting mirror is composed by 7 layers interleaving high refractive index ($PbSe$) layer and low refractive index (BaF_2) layer where the thickness of each layer has been fixed to quarter of a 6.2 µm-wavelength. This structure is similar to the one given in [6] where a thin SiO_2 layer is used for graphene deposition with chemical vapor deposition technique [13].

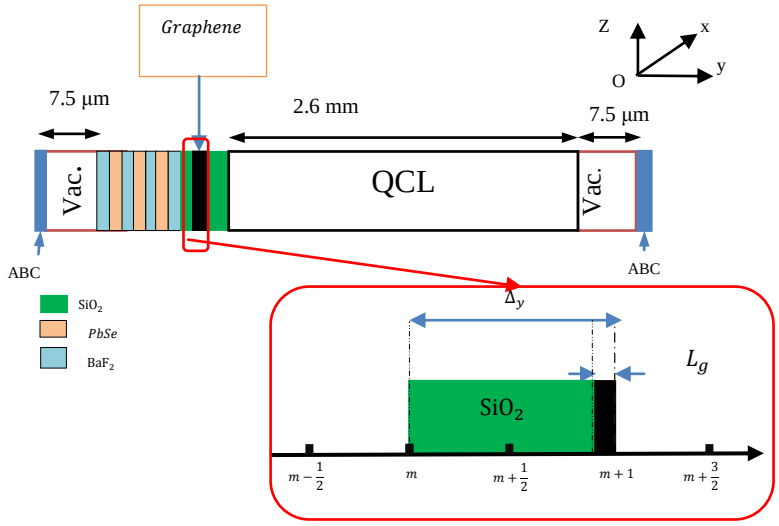

Figure 1: QCL 1-D structure integrating graphene and Bragg reflector.

The simulation parameter of graphene is summarized in Table 1. We used a QCL topology based on a diagonal transition with physical parameters similar to those given in [4]. In this structure, the upper and lower state wave functions are spatially localized in different regions and then the electron depopulation process is performed diagonally. The longitudinal relaxation time is high and close to 50 ps which is of the order of the round-trip time of the 3mm length laser cavity. For the FDTD simulation, we fix $\Delta y = 31\ nm$ and $\Delta t = 10.33\ fs$ to satisfy the Courant stability condition.

Parameters	Symbol	Value
Saturation intensity	$I_s\left(\frac{MW}{cm^{-1}}\right)$	0.2
Saturable loss	$\alpha_s\ (m^{-1})$	2.32 10^7
Non-saturable loss	$\alpha_{ns}\ (m^{-1})$	2.09 10^6

Table 1: Main parameters used in simulation

5 Simulation results

Fig. 2 shows the simulation results after 200 round-trips of a passive mode locking of MIR QCL using graphene as a saturable absorber. We observe the generation of an isolated pulse per round-trip time for a DC pumping rate of 1.1 times the threshold value. Without GSAM, the mode locking fails and the QCL generates the continuous waves. The presence of graphene layer has been favored the generation of stable pulses.

However, when the injection current is increased until 3 times threshold value, we can observe the apparition of a second pulse per round-trip. This second pulse is generated because of the Spatial Hole Burning occurring in such QCL structure where the gain recovery time is short compared to the round-trip time. In this case, the intensity of the side peaks of the laser pulse becomes strong and saturate the graphene absorption mechanism. We can notice the increase in the electric filed level compared to the pumping condition near threshold.

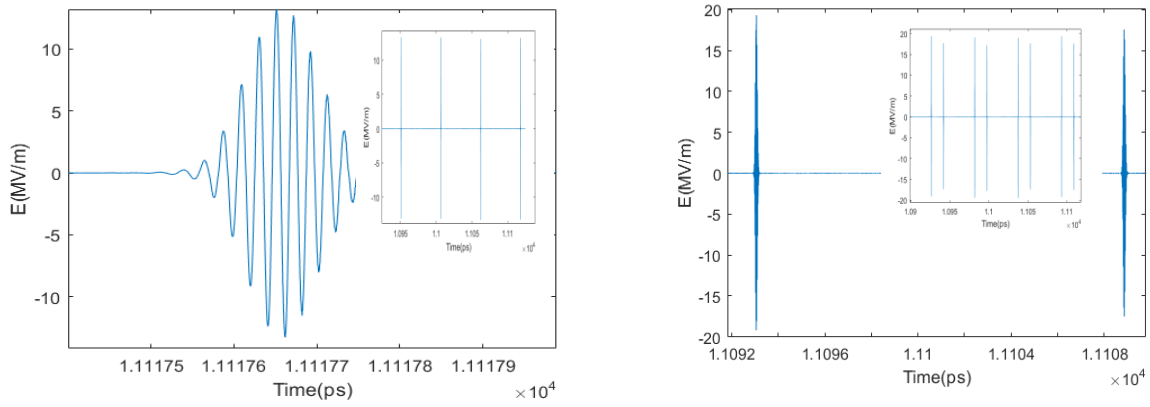

(a) (b)

Figure 2: Time evolution of the electric filed for pumping ratio (a) 1.1 and (b) 3 times the threshold value.

If we considered a vertical QCL structure characterized by a short longitudinal relaxation time of the order of picosecond, the gain recovery time is considerably small making the overlap with the short propagating pulses very weak. To analyze the effect of the longitudinal relaxation time on the mode locking behavior, we reduced T_1 to 5 ps. In Figure 3, we represent the simulation results for the pumping rate $a_p = 1.1$. We can observe the presence of multiple pulse per round-trip because the output intensity of the QCL is higher than the saturation intensity of the graphene which is saturated several times per round-trip.

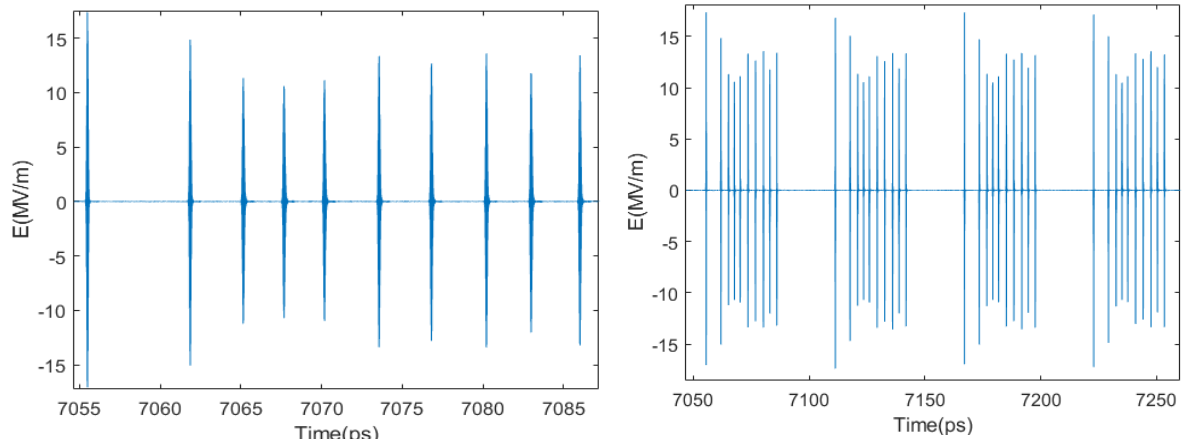

(a) (b)

Figure 3 : Time evolution of the electric filed for pumping ratio $a_p = 1.1$ and $T_1 = 5ps$ (a) single pulse and (b) a time window of the last 4th round-trips.

The overlap with pulse propagation and the QCL gain with short recovery time can be optimized with the length of the laser cavity. As it is known, the effect of the SHB is highly characterized with the level of DC pumping and the establishment of standing waves in the cavity. Thus, the length of the cavity is a non-negligible parameter that influences the laser dynamic. The round-trip time can be adjusted to limit the apparition of multiple pulses. For this, we have been tuned the cavity length to analyze this effect. Figure 4 represents the simulation results for pumping ratio $a_p = 1.1$ and cavity length of 1.63 mm. We can observe a significant reduce in SHB effect compared to the 2.6 mm cavity length. The maximum electric field of the generated pulse is not affected by the cavity length but prevents the appearance of other pulses through GSAM saturable absorber.

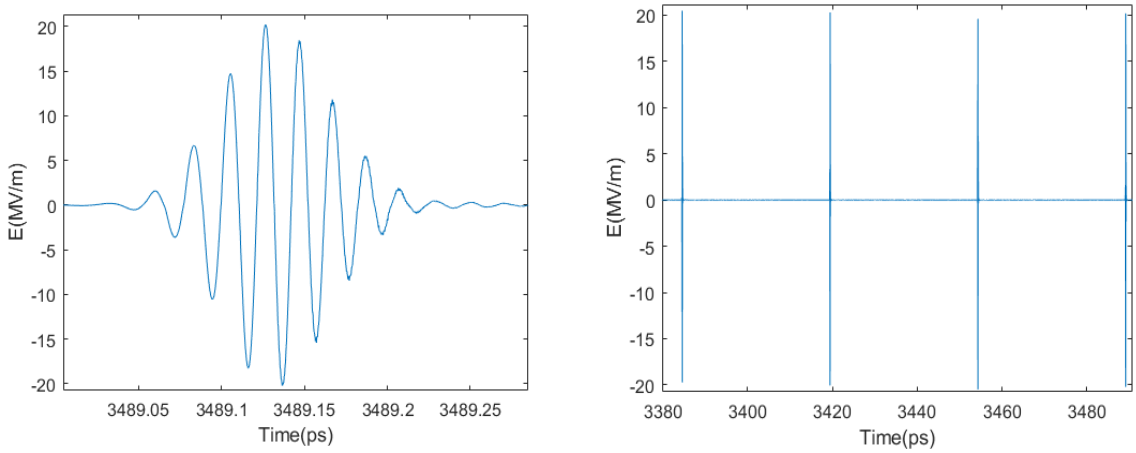

(a) (b)

Figure 4: Time evolution of the electric filed for pumping ratio $a_p = 1.1$, $T_1 = 5ps$ and L=1.63 mm (a) isolated pulse and (b) a time window containing four pulses.

6 Conclusion

In this work, we demonstrated the ability of passive mode locking of MIR QCL by incorporating a single-layer graphene as a saturable absorber using the FDTD method. The QCL is modelled by Maxwell-Bloch equations and graphene by Maxwell's equation through a nonlinear conductivity. The use of a high reflection mirror associated with graphene allows to increase the internal electric field magnitude due to the interference of the incident and reflected light at the mirror side. We observed a stable mode locking with the generation of an isolated pulse per round-trip for a DC pumping rate lower than 3 times the threshold value for QCL structures having a diagonal transition ($T_1 = 50\text{ps}$). Higher than this pumping rate, multiple pulses appear because they have reached the saturation intensity of the graphene. We simulated the QCL having a relaxation time $T_1 = 5\text{ps}$ corresponding to vertical transition structures. The obtained results show the presence of multiple pulses for a DC pumping close to threshold. This is due to SHB effect which become more significant when the gain recovery time is small compared to the round-trip time. By reducing the length of the cavity to 1.63 mm, a stable mode locking has been obtained through GSAM saturable absorption. This analysis should be improved with the consideration of different physical parameters of graphene in MIR spectrum.

Références bibliographiques

[1] J. Faist, F. Capasso, D. L. Sivco, C. Sirtori, A. L. Hutchinson, and A. Y. Cho, "Quantum Cascade Laser," *Science (80-.).*, vol. 264, no. 5158, pp. 553–556, Apr. 1994, doi: 10.1126/science.264.5158.553.

[2] E. P. Ippen, "Principles of passive mode locking," *Appl. Phys. B Laser Opt.*, vol. 58, no. 3, pp. 159–170, Mar. 1994, doi: 10.1007/BF01081309.

[3] V.-M. Gkortsas *et al.*, "Dynamics of actively mode-locked Quantum Cascade Lasers," *Opt. Express*, vol. 18, no. 13, p. 13616, Jun. 2010, doi: 10.1364/oe.18.013616.

[4] C. Y. Wang *et al.*, "Mode-locked pulses from mid-infrared Quantum Cascade Lasers," *Opt. Express*, vol. 17, no. 15, p. 12929, Jul. 2009, doi: 10.1364/oe.17.012929.

[5] A. Taflove, S. C. Hagness, and M. Piket-May, "Computational Electromagnetics: The Finite-Difference Time-Domain Method," in *The Electrical Engineering Handbook*, Elsevier, 2005, pp. 629–670.

[6] A. Mock, "Modeling Passive Mode-Locking via Saturable Absorption in Graphene Using the Finite-Difference Time-Domain Method," *IEEE J. Quantum Electron.*, vol. 53, no. 5, pp. 1–10, Oct. 2017, doi: 10.1109/JQE.2017.2732399.

[7] J. G. Maloney and G. S. Smith, "The efficient modeling of thin material sheets in the finite-difference time-domain (FDTD) method," *IEEE Trans. Antennas Propag.*, vol. 40, no. 3, pp. 323–330, Mar. 1992, doi: 10.1109/8.135475.

[8] R. W. Ziolkowski, J. M. Arnold, and D. M. Gogny, "Ultrafast pulse interactions with two-level atoms,"

Phys. Rev. A, vol. 52, no. 4, pp. 3082–3094, Oct. 1995, doi: 10.1103/PhysRevA.52.3082.

[9] F. T. Vasko, "Saturation of interband absorption in graphene," *Phys. Rev. B*, vol. 82, no. 24, p. 245422, Dec. 2010, doi: 10.1103/PhysRevB.82.245422.

[10] K. S. Yee, "Numerical Solution of Initial Boundary Value Problems Involving Maxwell's Equations in Isotropic Media," *IEEE Transactions on Antennas and Propagation*, vol. 14, no. 3. pp. 302–307, May 1966, doi: 10.1109/TAP.1966.1138693.

[11] J. G. Maloney and G. S. Smith, "The Efficient Modeling of Thin Material Sheets in the Finite-Difference Time-Domain (FDTD) Method," *IEEE Trans. Antennas Propag.*, vol. 40, no. 3, pp. 323–330, Mar. 1992, doi: 10.1109/8.135475.

[12] E. Dlala, A. Belahcen, and A. Arkkio, "A fast fixed-point method for solving magnetic field problems in media of hysteresis," *IEEE Trans. Magn.*, vol. 44, no. 6, pp. 1214–1217, 2008, doi: 10.1109/TMAG.2007.916673.

[13] D. Q. McNerny *et al.*, "Direct fabrication of graphene on SiO 2 enabled by thin film stress engineering," *Sci. Rep.*, vol. 4, pp. 1–9, 2014, doi: 10.1038/srep05049.